Progress In Electromagnetics Research, Vol. 119, 279–298, 2011

INVESTIGATION OF LOW-GRAZING-ANGLE MICROWAVE BACKSCATTERING FROM THREE-DIMENSIONAL BREAKING SEA WAVES

W. Luo[1], M. Zhang[1,*], C. Wang[2], and H.-C. Yin[2]

[1]School of Science, Xidian University, Xi'an 710071, China

[2]Science and Technology on Electromagnetic Scattering Laboratory, Beijing 100854, China

Abstract—The microwave backscattering of the sea surface is investigated with the wedge-shaped breaking waves for the super events at low grazing angles (LGA). According to the relationship between the wave breaking and the whitecap, the finite three-dimensional wedges are utilized to approximately model the breaking waves, of which the spatial distribution is simulated with whitecap coverage. The phase-modified two-scale method (TSM) and method of equivalent currents (MEC) are used to calculate the surface and volume scattering of sea surface and breaking waves respectively. The sea spikes in LGA are observed by this model, and the strong directionality is caused by the breakers. Considering the Bragg phase velocity, orbital motion of facets and wind drift, the Doppler spectrum is simulated with the time series of sea clutter. Included the breaking waves, the scattering model indicates that the enhanced non-Bragg scattering leads to the extended Doppler spectrum width. The numerical results agree with the measured data well at LGA. Compared with the statistical models, the complex physical mechanism of the sea scattering is explicitly described in this paper.

1. INTRODUCTION

The study of the electromagnetic scattering from the sea surface in low grazing angles (LGA) is of significance for remote sensing, surveillance and high solution radar imaging of the ocean [1–5]. Although the sea surface scattering is successfully modeled based on the Bragg theory in small and moderate incidence angles [6–13], some discrepancies

Received 26 June 2011, Accepted 25 July 2011, Scheduled 5 August 2011

* Corresponding author: Min Zhang (mzhang@mail.xidian.edu.cn).

between the predictions and experiment observations still cannot be explained. The terminology "super events" refers to the special phenomenon observed from the measured sea clutters, which includes sea spikes [14], polarization independence [15], faster scatters [16] and expanded width of Doppler spectrum [17].

It was observed that the sea spikes and Doppler spectrum peaks occurred associated with the wave breaking during the environmental measurements from the SAXON-CLT experiment [17]. Based on experiment data obtained in different sea environments Lee et al. [18] and Walker [19] analyzed the electromagnetical scattering mechanism of sea surface respectively. Both of them suggested that the super events are closely related to the non-Bragg scattering attributed from the breaking waves in LGA, and presented proper formula expressions.

Recently, the numerical scattering models of breaking waves are sorted into two categories. The first kind expends the geometrical models of breaking waves into sea surfaces and calculates scattering field with computational electromagnetics methods. The second kind calculates the total scattering coefficients of the sea surface and breaking waves with whitecap coverage in a statistical sense. West and Zhao generated breaking waves with the LONGTANK and combined the breaking waves with the sea surfaces inversed from the sea spectrum [20–22]. The large-scale breaking waves scattering was treated with the method of moment (MoM), Extended GO and three-dimensional multilevel fast-multipole algorithm (MLFMA). Kudryavtsev et al. [23] calculated the distributed surface scattering with the two-scale method (TSM) and take into account the modulation of the non-Bragg scattering, which is proportional to the whitecap coverage of the surface. This scattering numerical model agrees with the measured data in specific sea conditions properly.

According to the measured data and the photographs of the sea surface at LGA, Kalmykov and Pustovoytenko assumed that the wedges could approximate the sharp crests, which led to the increase of polarization ratio (HH/VV) [24]. Kwoh and Lake also suggested that the dominant scattering from the wave crest could be approximated by wedge scattering and analyzed the relationship of scattering fields from capillary wave and the wedge-shaped crest with small perturbation method (SPM) and geometrical theory of diffraction (GTD) respectively [25]. The dihedral wedge was consequently used to simulate the breaking wave, and the effect of the geometric parameters on the scattering was discussed with numerical methods [26–28]. Different from the breaking wave models simulated based on the hydrodynamic theory, the wedge model is simple and feasible for the analysis of sea surface scattering.

In this paper, the LGA backscattering of breaking sea waves is numerically modeled. The composite geometric model of the sea surface and wedge-like breaking wave is described in Section 2. While the TSM is modified with additional phase term, the non-Bragg scattering of breaking waves is investigated in Section 3. Furthermore the Doppler spectrum of the sea clutter is simulated for the measured data at LGA. Section 4 compares the numerical results with the experimental data and other methods, and some conclusions are presented in Section 5.

2. GEOMETRIC MODEL

2.1. Two-dimensional Sea Surface

The simulation of the sea surface fluctuation is essential for the model of time-varying electromagnetic scattering from ocean-like surface. If nonlinear wave interaction is neglected, the sea surface is assumed as superposition of harmonics whose amplitudes are independent Gaussian random variables with variances proportional to a certain sea spectrum $\psi(k_x, k_y)$. The linear sea surface is generated as follows. The white noise is firstly Fourier transformed into frequency domain and filtered by the sea spectrum. Then the height fluctuation $\zeta(\mathbf{r}, t)$ is obtained by the inverse fast Fourier transform (IFFT)

$$\zeta(\mathbf{r}, t) = \frac{1}{L_x L_y} \mathcal{F}^I \left[F\left(k_x,\, k_y\right) \right] \tag{1}$$

where the size of the sea surface is denoted with L_x and L_y, and the complex amplitude $F(k_x, k_y)$ is given as

$$F\left(k_x, k_y\right) = \xi 2\pi \sqrt{L_x L_y \psi\left(k_x, k_y\right)} \exp\left(j\omega_0 t\right) \tag{2}$$

ξ is a complex Gaussian process with zero mean and unity standard deviation, and ω_0 is the angular frequency of the sea wave propagation. In order to keep $\zeta(\mathbf{r}, t)$ as a real number, the phase of the Fourier coefficients should satisfy $F(K_x, K_y) = F^*(-K_x, -K_y)$ and $F(K_x, -K_y) = F^*(-K_x, K_y)$. The superscript "*" denotes conjugated complex number.

The JONSWAP spectrum [29] is used in this paper

$$\psi(\omega) = \alpha g^2 \frac{1}{\omega^5} \exp\left[-\frac{5}{4} \left(\frac{\omega_0}{\omega} \right)^4 \right] \cdot \gamma^{\exp\left[-\frac{(\omega-\omega_0)^2}{2\sigma^2\omega_0^2} \right]} \tag{3}$$

where ω is the frequency of the sea wave and α is the dimensionless constant which is related to the wind speed U_{10} at a height of 10 m. Other parameters can be referred in [29]. Considering the wind

direction, the directional factor $G(\omega, \varphi)$ is introduced and Equation (3) is rewritten as

$$\psi(k_x, k_y) = \psi(\omega, \varphi) = \psi(\omega) \cdot G(\omega, \varphi) \tag{4}$$

$$G(\omega, \varphi) = \begin{cases} (2/\pi)\cos^2(\varphi - \varphi_\omega) & -\pi/2 + \varphi_\omega < \varphi < \pi/2 + \varphi_\omega \\ 0 & \theta \geq \pi/2 + \varphi_\omega, \ \ \varphi \leq -\pi/2 + \varphi_\omega \end{cases} \tag{5}$$

where φ is the observation direction, and φ_ω is the wind direction. In the calculations above, the dispersion relationship $\omega = \sqrt{gk\,(1 + k^2/k_m^2)}$ must be satisfied. It should be stressed that the discretization in the sea spectrum and space domain should follow the sampling theorem. Since the energy domain of the sea spectrum depends on wind speed, the selected range of sea spectrum should contain the dominant energy domain of the sea surface.

2.2. Wedge-like Breaking Wave

In real sea conditions the scattering field of short sea waves is running along the longer surface waves, and the Bragg scattering loses validity. According to the photographs and data taken in the field experiments [14, 24], the single sharply crested unbroken wave can be approximately simulated with the dihedral wedge of finite length shown in Figure 1. Different from the infinite two-dimensional wedge in the previous literatures, the dihedral wedge is characterized by internal angle β, length d, width $2l$ and height h. Since the size of the wave crest is related to incidence microwave, d and $2l$ are presented in wavelength of incidence wave λ. Supported by observations and the Stokes' theory, the internal angle β is 120°. The polarization characteristic of the wedge scattering can properly simulate the unbroken sharp wave crests.

The evolution of breaking waves is investigated in experiments [30] and with numerical tank [31] in detail. With increasing wind speed, the nonlinearity of the wave fluctuation keeps stronger. When and only when the horizontal water particles velocity reaches $d\omega/dk$, wave breaking occurs inevitably in a short time, usually within a quarter of a wave period. During the last stage of the wave breaking, waves experience strong deformations: greater steepness, front face steeping and a jet forming at the crest [31]. Then the whitecaps are generated after the stage of surging breakers.

For the sake of complex generation process of breaking wave, it is difficult to model the spatial distribution of the breakers on the sea surface explicitly. Whereas the statistical study of the probability of wave breaking has been fully developed [32, 33]. Recently, the criterions of the wave breaking are the geometrical criterion, kinematic criterion and dynamic criterion, which can be transformed into each other with

mathematical derivation. The whitecap coverage q can be expressed with probability density function $f(\eta_x)$ [32]

$$q = \frac{1}{2}\int_{-\infty}^{-\eta} f(\eta_x)\, d\eta_x \tag{6}$$

η_x is the slope of the sea surface, and η is the slope criterion. The waves will be broken at the point where the sea slope is higher than variable η. Since the wave crests which are to be transformed into whitecaps is of interest for us, the slope criterion η of the whitecap is used to locate the breaking waves. Then the wedge-like breaking waves are set at the breaking point, and the composite geometrical model including sea surface and breaking waves is established.

In order to verify the breaker distribution in this paper, the simulated coverage with slope criterion is compared with the

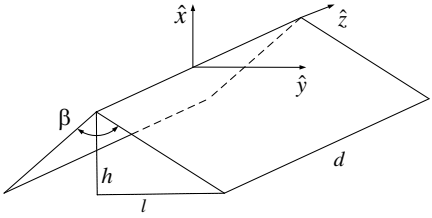

Figure 1. Wedge model of crested wave.

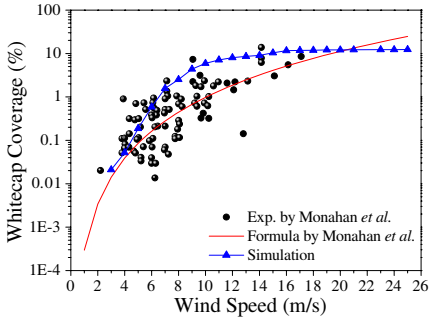

Figure 2. Breaker coverage versus wind speed.

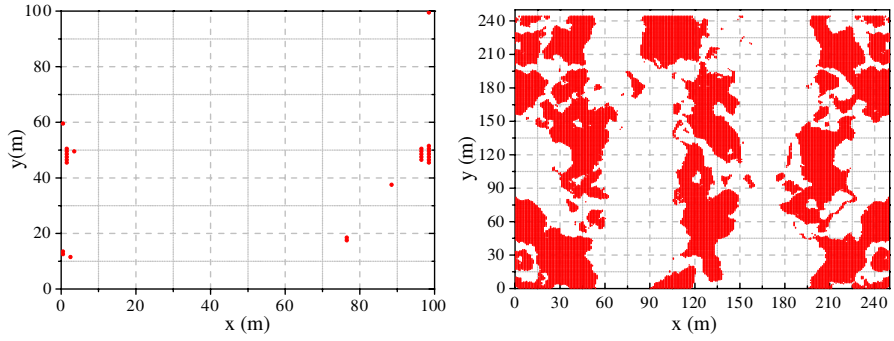

Figure 3. Spatial distribution of breaking waves on the sea surface. (a) $U_{10} = 8\,\mathrm{m/s}$, (b) $U_{10} = 20\,\mathrm{m/s}$.

measured coverage and the empirical results from Monahan and Muircheartaigh [33] in Figure 2. Due to the agreements of the simulated coverage with experimental data and empirical formula, $\eta = 0.586$ proves to be reasonable. It is noted that the whitecap coverage reach 12% under 20 m/s wind speed condition, which indicates the significant impact of the breaking waves on the scattering of sea surface. Modeled with slope criterion $\eta = 0.586$, the spatial distribution of the breaking waves is shown in Figure 3. The breakers are randomly distributed on the sea surface, of which the coverage area increases with wind speed.

3. COMPOSITE SCATTERING MODEL INCLUDING BREAKING WAVES

3.1. Phase-modified Two-scale Method

In the high frequency bands, the TSM [34] is used for the calculation of sea surface scattering, which reckons that the waves contributing to the Bragg process are locally tilted by large-scale waves [35]. The two scale scattering coefficient is simply a weighted average of the local small perturbations coefficients, the weight being proportional to the probability of the slope's probability distribution. The classical scattering coefficient of sea surface is formulated as

$$\sigma_{pq}^{0}(\theta_i) = \int_{-\infty}^{\infty} \int_{-\cot\theta_i}^{\infty} \sigma_{pq}^{\mathrm{SPM}}\left(\theta_i'\right)\left(1 + z_x \tan\theta_i\right) P\left(z_x', z_y'\right) dz_x dz_y \qquad (7)$$

$\sigma_{pq}^{\mathrm{SPM}}\left(\theta_i'\right)$ is the SPM solution to the scattering from the small scale. θ_i and θ' are the incidence angles in global and local reference frames, respectively. p and q denote incidence and scattering polarizations. $P(z_x', z_y')$ is the slope probability density function as viewed from the incidence direction. The modulation of large-scale roughness on the small-scale counterpart is operated with the integral on the sea surface slope.

Since the sea surface model is discretized with triangular facets in this paper, $P(z_x', z_y')$ can be removed, and Equation (7) is rewritten as

$$\sigma_{pq}^{0}(\theta_i) = \frac{1}{M}\frac{1}{N}\sum_{m=1}^{M}\sum_{n=1}^{N} \sigma_{pq}^{\mathrm{SPM}}(\theta_i')\ \left[1 + z_x(x_m, y_n)\tan\theta_i\right] \qquad (8)$$

The superposition of the scattering contribution from the facets substitutes the integral of slope. M and N are the sampling number of the sea surface model. $z_x\left(x_m, y_n\right)$ is the slope of the sampling point (x, y) in x direction.

The classical TSM only gives sea scattering intensity with Equation (7). In order to analyze the Doppler spectrum of the sea clutter, the phase information of the scattering field is necessary. Considering both the phase shifts associated with the traveled path distance and the reflection coefficients for each scattering facet, the classical TSM is modified with modified facet phase. As shown in Figure 4, the facets should be large enough for electromagnetic wavelength and small enough to characterize the phase variation of the surface fluctuation. With additional phase ϕ_{add}, the scattering field is obtained based on Equation (8)

$$E_{pq}^{\mathrm{TSM}} = \frac{1}{M}\frac{1}{N}\sum_{i=1}^{M}\sum_{j=1}^{N}\sqrt{I_{ij}\Delta S}\exp\left(j\phi_{add}\right) \tag{9}$$

$$I_{ij} = \sigma_{pq}^{\mathrm{SPM}}(\theta_i')\left[1 + z_x(x_m, y_n)\tan\theta_i\right] \tag{10}$$

$$\phi_{add} = \xi\cdot\varphi_{\max} + (\mathbf{k}_i - \mathbf{k}_s)\cdot\mathbf{r} \tag{11}$$

I_{ij} and ΔS are the scattering intensity and area of single facet respectively. $\varphi_{\max}$ is the maximum of the phase difference in the facet, and ξ is a random number between -0.5 and 0.5 ($\xi \in [-1/2, 1/2]$). $\mathbf{r}$ is the location of the facet in the global reference frame, and $(\mathbf{k}_i - \mathbf{k}_s)\cdot\mathbf{r}$ presents the phase delay caused by the relative position of the facets.

3.2. Non-Bragg Scattering of Breaking Wave

For the sake of the enhanced roughness of the sea surface and the breaking waves, the non-Bragg scattering is of significance at LGA, which is closely related to the super events. According to the sea spikes in high-resolution radar observation and large deviations of the observed polarization ratio, it is recognized that the two-scale method cannot fully explain the radar signature with the Bragg theory at large incidence angles ($\theta_i > 30^\circ$). The volume scatters on the sea surface are generally considered as the source of non-Bragg scattering.

Based on the energy balance equation, Kudryavtsev et al. [23] proposed a simplified scattering model

$$\sigma_k(\theta,\varphi) = \sigma_{br}(\theta,\varphi)(1-q) + \sigma_{wb}(\theta,\varphi) \tag{12}$$

The full model of scattering coefficient is σ_k, which is the sum of the Bragg component σ_{br} and of the non-Bragg component σ_{wb}. While σ_{br} is the scattering coefficient calculated with TSM, σ_{wb} is the modulated scattering of the areas covered by plumes (spilling breakers). This is apparently a weighted average of σ_{br} and σ_{wb} with the whitecap coverage q.

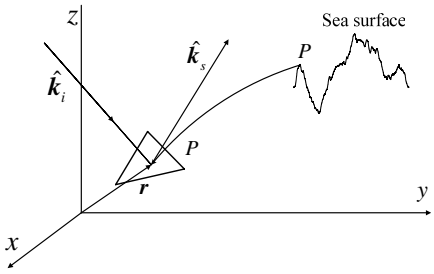

Figure 4. Facets of the sea surface.

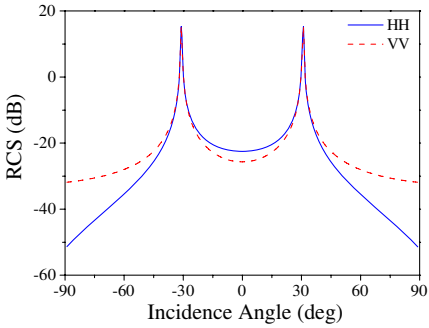

Figure 5. Backscattering RCS of the single wedge versus the incidence angle.

Since Equation (12) only gives the statistical scattering coefficient of the full model, the wedge scattering is adopted for the simulation of the scattering from breaking waves in this paper. The wedge scattering has been fully studied with diffraction theories. This paper uses the method of equivalent currents (MEC) [36] to calculate wedge scattering field E_{pq}^{wedge}

$$E_{pq}^{\text{wedge}}=jk_0\int_C\left[\eta_0 I\left(r'\right)\hat{k}_s\times\left(\hat{k}_s\times\hat{t}\right)+M\left(r'\right)\left(\hat{k}_s\times\hat{t}\right)\right]\frac{\exp\left(-jk_0 s\right)}{4\pi s}dl \quad (13)$$

I and M, which are the equivalent edge electrical current and magnetic current (EEC) flowing along the edge respectively, have three major types [37]. The GTDEEC, which involves both diffraction and PO reflection fields, is chosen in this paper.

Electromagnetically, the edge of the wedge acts as an impedance discontinuity to currents induced in a direction normal to the edge, which is responsible for the difference of scattering of the HH and VV polarizations. The backscattering radar cross sections (RCS) of a single wedge and incidence angle are compared in Figure 5. The incidence wave is 10 GHz, and the geometric parameters of the wedge are: $l = 5\lambda$, $d = 12\lambda$. The two peaks are caused by the specular reflection of the wedge plane. The HH polarized RCS is higher than its VV counterpart between the two peaks, which indicates that polarization features of the wedge scattering is similar to those of the sharp-crested waves.

Based on the composite geometric model in Section 2, the Bragg scattering is calculated with phase-modified TSM, and the non-Bragg scattering is approximately simulated with the coherent summation of

scattering fields from the wedges located at the breaking points. Then the total scattering field of the composite model is written as

$$E_{pq}^{\text{total}} = E_{pq}^{\text{TSM}} + \sum_{i=1}^{num} E_{i,pq}^{\text{wedge}} \tag{14}$$

3.3. Doppler Spectrum

Since the Doppler analysis proves to be a much more precise and sensitive tool in assessing the validity of scattering model than the usual comparison of RCS, the Doppler spectrum of the sea clutter is of interest for the remote sensing in the sea environment.

According to the Bragg scattering theory, the capillary sea wavenumber K_{B} and the microwave wavenumber k satisfy the relationship

$$K_{\text{B}} = 2k \sin \theta_i \tag{15}$$

For deep water, the Bragg phase velocity c_{B} of the gravity-capillary wave is given as

$$c_{\text{B}} = \sqrt{\frac{g}{K_{\text{B}}} + \varsigma \frac{K_{\text{B}}}{\rho}} \tag{16}$$

where g is the acceleration of gravity, ς is the surface tension and ρ is the density of sea water. It is apparent that c_{B} rests with the incidence angle and microwave frequency, and is independent of the wind speed and polarization. The classical model of the sea clutter Doppler spectrum is only suitable for a small incidence angle and cannot interpret some special events in high wind speed and low grazing angles. The frequency shift of the measured Doppler spectrum is usually larger than simulated ones, which is different from Bragg scattering theory. Moreover, the separation of HH and VV polarized Doppler spectrums is observed in real sea experiments. According to Bragg theory, the width of Doppler spectrum decreases with the increase of incidence angle. However, the larger spectrum width is found in the measured data.

Therefore, the non-Bragg scattering is introduced to account for the special events aforementioned. With increasing wind speed, the shapes of the sea waves become more trochoidal, and the motions of the facets on the sea surface are no longer closed orbits. Thus the Stokes solution to the wave equation should be included to describe the cycloidal movement of the water particles. For open waters, such as sea surface, the drift currents at depth d is given as [38]

$$v_c = \Omega K_p \left(\frac{H}{2}\right)^2 \frac{\cosh(2K_p d)}{2\sinh^2(K_p d)} \tag{17}$$

where Ω and K_p are the angular frequency and wavenumber of the dominant wave, respectively. The wave height is denoted as H.

The wind drift is directly related to the breaking waves. Research has shown a good approximation to the wind drift velocity v_w [16]

$$v_w = \alpha U, \quad \alpha = 2.6 - 5.5\%. \tag{18}$$

Although the scattering environment of sea surface is complex, the Doppler frequency shift is basically determined by c_{B}, v_c and v_w. According to the definition of Doppler spectrum, the up-down motions of the surface facets and breaking waves are assumed as the cause of broadened spectral width in real sea conditions in this paper. The relationship of the spectral width with breaking waves is discussed in Section 4.

For the time-varying composite scattering model, the Doppler spectrum is calculated with a standard spectral estimation technique [39]

$$S_a(f) = \langle S(f) \rangle \tag{19}$$

$$S(f) = \frac{1}{T} \left| \int_0^T E^{sc}(t, \theta_s; \theta_i) \exp(-j2\pi f t)\, dt \right|^2 \tag{20}$$

$S(f)$ is the periodogram of the scattering field E^{sc} which is vertical polarization (TM) or horizontal polarization (TE). $S_a(f)$ is the assemble average of $S(f)$. And 100 time-evolving surface realizations are used in this paper.

4. NUMERICAL RESULTS

The modified composite scattering model including the breaking wave is compared with the measured data and the TSM in Figure 6. The measured data used were collected from moderate incidence angles to low grazing angles at Ku band (14 GHz) in 1991 [40]. According to the numerical models of breaking wave [20], the geometric parameters of the wedge are set as $l = 5\lambda$, $d = 12\lambda$. Both HH and VV polarization backscattering coefficients are compared under different wind speeds. The parameters of the wedge prove to be reasonable for the agreements of the composite model with the measured data.

The under-prediction of σ_{HH} by TSM is apparent in Figures 6(a) and (c). While the discrepancy of TSM and the modified composite model is inconspicuous in moderate incidence angles, significantly enhanced σ_{HH} is found from the modified composite model in LGA. At 13 m/s wind speed, σ_{HH} is close and even equal to σ_{VV} in some incidence angles, which is referred as polarization independence. The strong increase of HH polarized scattering is obviously related to

sea spikes. It is also noted that VV polarized Bragg scattering is still dominant in large angles shown in Figures 6(b) and (d), which is properly predicted by tilting modulation of Bragg roughness. In addition, the numerical results are consistent with the PDF of the normalized cross-section at LGA in [41].

The Ku band (14 GHz) composite backscattering including breakers is compared with the Kudryavtsev model [23] under 15 m/s wind speed in Figure 7. Both of the models predict the enhancement of HH polarization in LGA and yield similar results in moderate incidence angles. Since Kudryavtsev model does not consider the polarization features of non-Bragg scattering, the contribution from the breakers just depends on whitecap coverage W. It is consequently found that the Kudryavtsev model is higher than our model in HH polarization and weaker than our model in VV polarization.

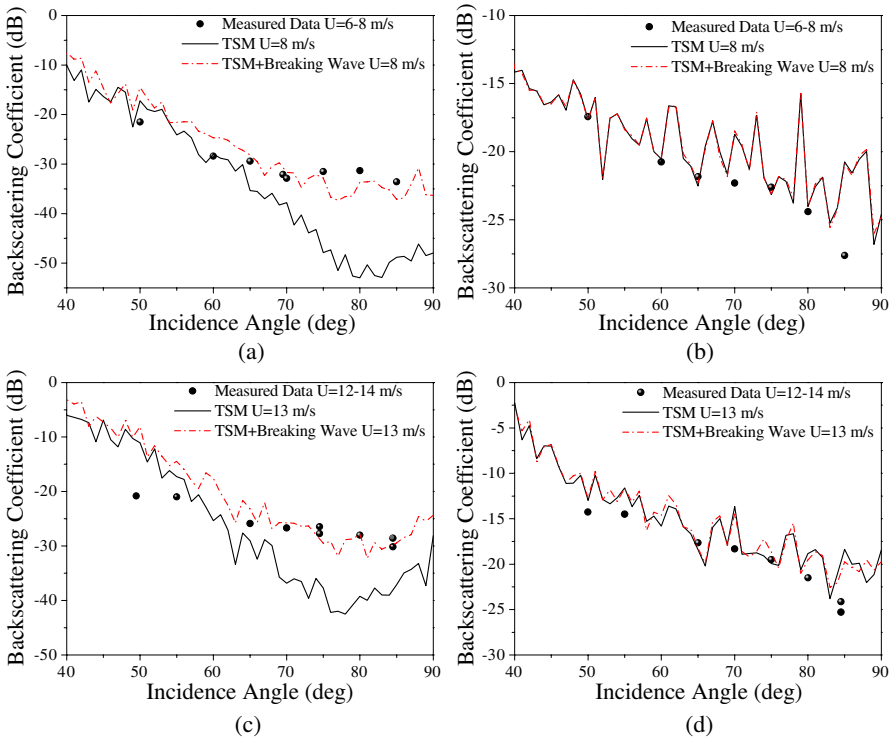

Figure 6. Backscattering coefficient versus the incidence angle in different wind speeds. (a) HH polarization, (b) VV polarization, (c) HH polarization, (d) VV polarization.

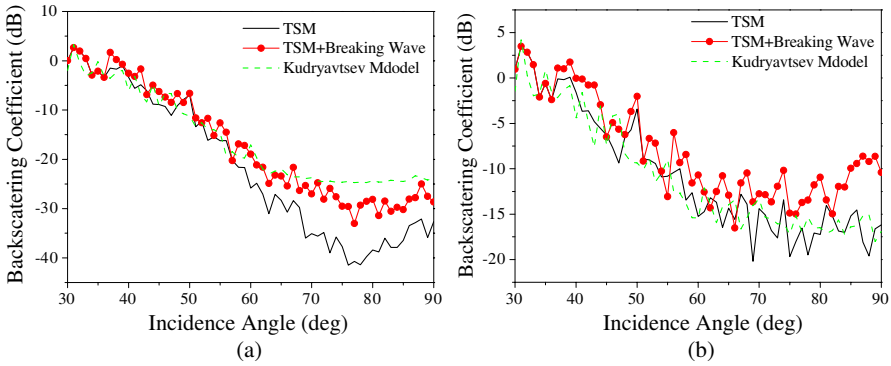

Figure 7. Comparison of composite scattering including breakers and the kudryavtsev model under $U_{10} = 15\,\mathrm{m/s}$ wind speed. (a) HH polarization, (b) VV polarization.

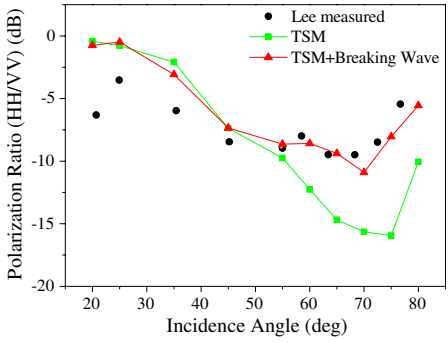

Figure 8. HH/VV Polarization ratio versus the incidence angle.

The influence of breakers scattering on polarization ratio is shown in Figure 8, along with previous published measurements data of the ocean [16]. The experiment is conducted at X band, and the wave direction is upwind. The wind speed varies with the incidence angle. Although Figure 8 shows the HH polarized scattering is weaker than the VV counterpart in each incidence direction, the strong increase of polarization ratio (HH/VV) in LGA proves the existence of non-Bragg scattering, which is referred as "fast signals" in [16]. Different from the classical TSM, the modified composite model agree with the measured data closely.

It is known that the wind-driven sea surface is anisotropy, and the discrepancy of the up wind and down wind is especially apparent. However, the azimuth angle distribution of the backscattering

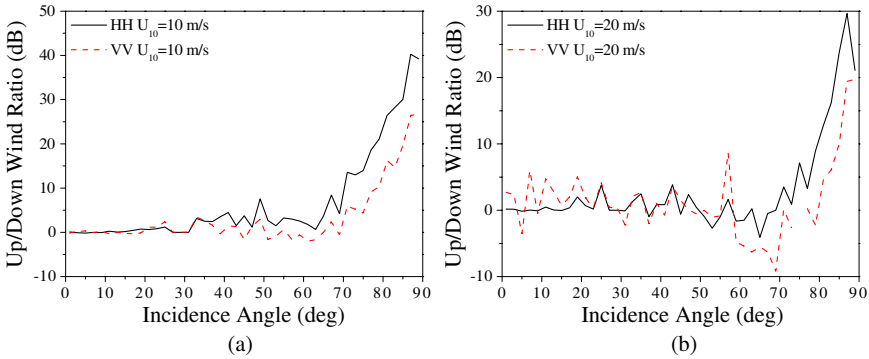

Figure 9. Up/Down wind ratio ($\sigma_{\rm up}/\sigma_{\rm down}$) versus the incidence angle. (a) $U_{10} = 10\,{\rm m/s}$, (b) $U_{10} = 20\,{\rm m/s}$

coefficient with classical TSM is symmetric because of the lack of volume scattering. The up/down wind ratio ($\sigma_{\rm up}/\sigma_{\rm down}$) is introduced to discuss the directional characteristics of the composite scattering with breaking waves in Figure 9. The ratio almost keeps invariant in small and moderate incidence angles but is steeply peaked in the large incidence angles. The HH polarized up/down wind ratio is much higher than the VV counterpart in LGA, which indicates the apparent directionality of breaking waves. Furthermore, $\sigma_{\rm up}/\sigma_{\rm down}$ in 20 m/s wind speed is lower than the one in 10 m/s. Thus the directionality of scattering from the breaking waves is weakened by the wind speed.

The simulated Doppler spectrums including breaking waves are compared with the measured time-integrated Doppler spectra of wind waves [16] in Figure 10. The operating frequency of the microwave scatterometer is in X band, and the incidence angle varies from 35° to 80°. The upwind direction is considered, and the wind speed slightly varies with incidence angle. The two peaks of the simulated Doppler spectrums are pointed out in Figure 10, which are in accordance with the measured data. The lower peak indicates the slow scatter caused by Bragg shift and orbital motion, and the higher one indicates the fast scatter caused by wind drift.

Since the spectrum is inversed from the time series of sea clutter with fast Fourier transform (FFT), the phenomena that the HH spike exceeds the VV scattering amplitude cannot be found. Because of little contribution of the breakers to the scattering in $\theta_i = 35°$, the fast scatter peak is not simulated in Figure 10(a), which may be arisen by some special source in the experiments. As shown in Figure 10(c), there is a trough between the fast and slow scatters of the VV polarized

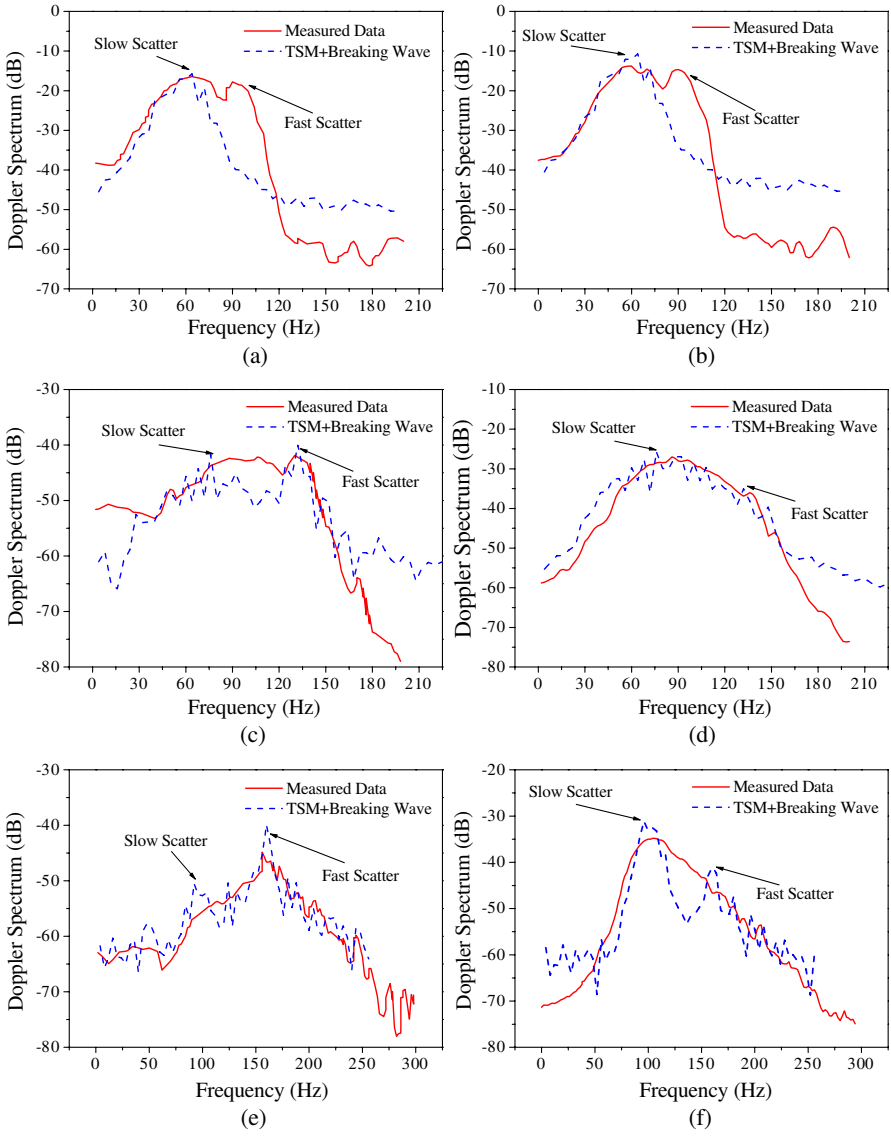

Figure 10. Comparisons of the simulated doppler spectrum with the measured data. (a) $\theta_i = 35°$, HH polarization, (b) $\theta_i = 35°$ VV polarization, (c) $\theta_i = 65°$, HH polarization, (d) $\theta_i = 65°$ VV polarization, (e) $\theta_i = 80°$, HH polarization, (f) $\theta_i = 80°$ VV polarization.

spectrum, which is caused by the deviation of the simulated vertical motion with the real sea surface. Reasonable agreements of simulated spectrum and measured data are found in other conditions.

Figure 10 shows that the scattering from breaking waves is dominant in HH polarization at LGA, and the peak of the sea surface scattering is concealed, which is a kind of super events. The spectral width is determined by the distance between the two peaks. Although the frequency shifts of the fast and slow scatters both increase with the incidence angle, the increment from fast scatter is much larger. The spectral width accordingly increases with incidence angle, which is accordance with the experiments in wave tank [42].

The simulated Doppler spectrums in different wind speed are shown in Figure 11. The incidence angle is 80°, and the frequency of the incidence wave is 14 GHz. For reference, the frequency shifts of the fast and slow scatters are shown in Table 1. Since the measured data in Figure 10 are obtained with scatterometer mounted on a boat, the frequency shift is enlarged by the boat velocity, which is excluded in Figure 11. The peak of the fast scatter obviously increases with the wind speed, while the increments of the slow scatter are inconspicuous. Thus the spectral width increases with the wind speed. It is also noted that the spectral amplitude of the fast scatter is much higher than the slow counterpart in HH polarization at LGA. It can be concluded that the non-Bragg scattering is much stronger than the Bragg scattering from the sea surface, and the frequency shift is sensitive to the wind speed in LGA.

Since the size of the wedge-shaped breakers is finite, the geometric parameters of the wedge are of significance for the sea surface scattering. While the slope criterion keeps 0.586, the number of breakers increases with wind speed. Although the width and length of the breakers in open sea surface have not been mentioned in previous literatures, the wave breaking has been simulated with the LONGTANK. The size of the wedge-shaped breakers keeps consistent with the numerical model of LONGTANK [20], and the agreements of the numerical results with measured data above prove the validity of the parameters.

Table 1. Doppler frequency shifts of the fast scatter and slow scatter in different wind speeds.

	$U_{10} = 10\,\mathrm{m/s}$	$U_{10} = 15\,\mathrm{m/s}$	$U_{10} = 20\,\mathrm{m/s}$
Fast Scatter (Hz)	46.26	63.40	80.54
Slow Scatter (Hz)	18.68	22.04	25.39

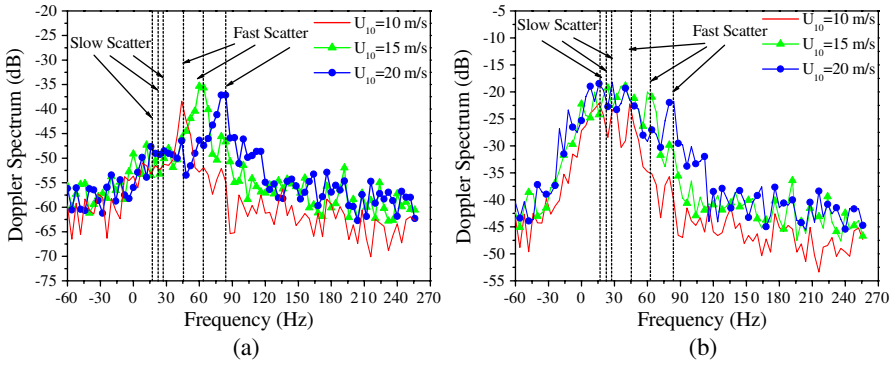

Figure 11. Simulated Doppler spectrum in different wind speeds. (a) HH polarization, (b) VV polarization.

5. CONCLUSION

A modified composite model including breaking waves, which is suitable for the microwave scattering at LGA, is proposed in this paper. Different from the previous numerical methods mentioned in Section 1, our model focuses on the simulation of electromagnetical scattering of realistic 2-D sea surface. The finite 3-D wedge-shaped breaking waves are considered as the source of non-Bragg scattering, and the simulated results of scattering coefficients and polarization ratio are in agreement with those in experiments. Furthermore, the intensity and phase of the time-varied scattering field are provided by our model, and the Doppler spectrum of the sea clutter is simulated, which is in accordance with the measured data. It is found that the non-Bragg scattering is dominant in scattering intensity distribution and Doppler spectrum at LGA. Considering the scattering features of the breakers, we explain the super events in LGA with the numerical results. Our model provides refined understanding of the sea surface backscattering at LGA and is helpful for the investigations of measured data of field experiments in the open ocean.

ACKNOWLEDGMENT

The authors would like to thank the National Natural Science Foundation of China for Grant No. 60871070, the National Pre-research Foundation and the Foundation of the National Electromagnetic Scattering Laboratory to support this kind of research.

REFERENCES

1. Zhang, M., Y. W. Zhao, H. Chen, and W.-Q. Jiang, "SAR imaging simulation for composite model of ship on dynamic ocean scene," *Progress In Electromagnetics Research*, Vol. 113, 395–412, 2011.
2. Luo, W., M. Zhang, Y. W. Zhao, and H. Chen, "An efficient hybrid high-frequency solution for the composite scattering of the ship on very large two-dimensional sea surface," *Progress In Electromagnetics Research M*, Vol. 8, 79–89, 2009.
3. Zhao, Y. W., M. Zhang, and H. Chen, "An efficient ocean SAR raw signal simulation by employing fast Fourier transform," *Journal of Electromagnetic Waves and Application*, Vol. 24, No. 16, 2273–2284, 2010.
4. Liang, D., P. Xu, L. Tsang, Z. Gui, and K.-S. Chen, "Electromagnetic scattering by rough surfaces with large heights and slopes with applications to microwave remote sensing of rough surface over layered media," *Progress In Electromagnetics Research*, Vol. 95, 199–218, 2009.
5. Chen, K.-S., L. Tsang, and J.-C. Shi, "Microwave emission from two-dimensional inhomogeneous dielectric rough surfaces based on physics-based two-grid method," *Progress In Electromagnetics Research*, Vol. 67, 181–203, 2007.
6. Mittal, G. and D. Singh, "Critical analysis of microwave specular scattering response on roughness parameter and moisture content for bare periodic rough surfaces and its retrieval," *Progress In Electromagnetics Research*, Vol. 100, 129–152, 2010.
7. Brelet, Y. and C. Bourlier, "SPM numerical results from an effective surface impedance for a one-dimensional perfectly-conducting rough sea surface," *Progress In Electromagnetics Research*, Vol. 81, 413–436, 2008.
8. Ishimaru, A., C. Le, Y. Kuga, L. A. Sengers, and T. K. Chan, "Polarimetric scattering theory for high slope rough surface," *Progress In Electromagnetics Research*, Vol. 14, 1–36, 1996.
9. Fabbro, V., C. Bourlier, and P. F. Combes, "Forward propagation modeling above Gaussian rough surfaces by the parabolic shadowing effect," *Progress In Electromagnetics Research*, Vol. 58, 243–269, 2006.
10. Xu, P., K.-S. Chen, and L. Tsang, "Analysis of microwave emission of exponentially correlated rough soil surfaces from 1.4 GHz to 36.5 GHz," *Progress In Electromagnetics Research*, Vol. 108, 205–219, 2010.
11. Chen, H., M. Zhang, D. Nie, and H.-C. Yin, "Robust semi-

deterministic facet model for fast estimation on EM scattering from ocean-like surface," *Progress In Electromagnetics Research B*, Vol. 18, 347–363, 2009.

12. Oraizi, H. and S. Hosseinzadeh, "A novel marching algorithm for radio wave propagation modeling over rough surfaces," *Progress In Electromagnetics Research*, Vol. 57, 85–100, 2006.
13. Chang, Y.-L., C.-Y. Chiang, and K.-S. Chen, "SAR image simulation with application to target recognition," *Progress In Electromagnetics Research*, Vol. 119, 35–57, 2011.
14. Lewis, B. L. and I. D. Olin, "Experimental study and theoretical model of high-resolution radar backscatter from the sea," *Radio Sci.*, Vol. 15, 815–828, 1980.
15. Fuchs, J., D. Regas, T. Waseda, S. Welch, and M. P. Tulin, "Correlation of hydrodynamic features with LGA radar backscatter from breaking waves," *IEEE Trans. Geosci. Remote Sens.*, Vol. 37, No. 5, 2442–2460, 1999.
16. Lee, P. H. Y., et al., "X band microwave backscattering from ocean waves," *J. Geophys. Res.*, Vol. 100, No. 2, 2591–2611, 1995.
17. Jessup, A. T., W. K. Melville, and W. C. Keller, "Breaking waves affecting microwave backscatter 1. detection and verification," *J. Geophys. Res.*, Vol. 96, No. C11, 20547–20559, 1991.
18. Lee, P. H. Y, et al., "Wind-speed dependence of small-grazing-angle microwave backscatter from sea surfaces," *IEEE Trans. Antennas Propagat.*, Vol. 44, No. 3, 333–340, 1996.
19. Walker, D., "Doppler modelling of radar sea clutter," *IEE Proceedings — Radar, Sonar and Navigation*, Vol. 148, No. 2, 73–80, 2001.
20. West, J. C. and Z. Q. Zhao, "Electromagnetic modeling of multipath scattering from breaking water waves with rough faces," *IEEE Trans. Geosci. Remote Sens.*, Vol. 40, No. 3, 583–592, 2002.
21. West, J. C., "Low-grazing-angle (LGA) sea-spike backscattering from plunging breaker crests," *IEEE Trans. Geosci. Remote Sens.*, Vol. 40, No. 2, 523–526, 2002.
22. Zhao, Z. Q. and J. C. West, "Low-grazing-angle microwave scattering from a three-dimensional spilling breaker crest: A numerical investigation," *IEEE Trans. Geosci. Remote Sens.*, Vol. 43, No. 2, 286–294, 2005.
23. Kudryavtsev, V., D. Hauser, G. Caudal, and B. Chapron, "A semiempirical model of the normalized radar cross-section of the sea surface 1.Background model," *J. Geophys. Res.*, Vol. 108, No. C3, 8054, 2003.

24. Kalmykov, A. I. and V. V. Pustovoytenko, "On polarization features of radio signals scattered from the sea surface at small grazing angles," *J. Geophys. Res.*, Vol. 81, No. 12, 1960–1964, 1976.
25. Kwoh, D. S. W. and B. M. Lake, "A deterministic, coherent and dual-polarized laboratory study of microwave backscattering from water waves, part I: Short gravity waves without wind," *IEEE Journal of Oceanic Engineering*, Vol. 9, No. 5, 291–308, 1984.
26. Lyzenga, D. R., A. L. Maffett, and R. A. Shuchman, "The contribution of wedge scattering to the radar cross section of the ocean surface," *IEEE Trans. Geosci. Remote Sens.*, Vol. GE-21, No. 4, 502–505, 1983.
27. Ericson, E. A. and D. R. Lyzenga, "Performance of a numerical iterative solution of the surface current integral equation for surfaces containing small radii of curvature," *Radio Sci.*, Vol. 33, No. 2, 205–217, 1998.
28. Lyzenga, D. R. and E. A. Ericson, "Numerical calculations of radar scattering from sharply peaked ocean waves," *IEEE Trans. Geosci. Remote Sens.*, Vol. 36, No. 2, 636–646, 1998.
29. Hasselmann, D. E., "Directional wave spectra observed during JONSWAP 1973," *J. Phys. Oceanogr.*, Vol. 10, No. 7, 1264–1280, 1980.
30. Lee, P. H. Y., et al., "Scattering from breaking gravity waves without wind," *IEEE Trans. Antennas Propagat.*, Vol. 46, No. 1, 14–26, 1998.
31. Wang, P., Y. Yao, and M. P. Tulin, "An efficient numerical tank for nonlinear water waves, based on the multi-subdomain approach with BEM," *Int. J. Numer. Meth. Fluids*, Vol. 20, 1315–1336, 1995.
32. Xu, D., X. Liu, and D. Yu, "Probability of wave breaking and whitecap coverage in a fetch-limited sea," *J. Geophys. Res.*, Vol. 105, No. C6, 14253–14259, 2000.
33. Monahan, E. C. and I. Ó Muircheartaigh, "Optimal power-law description of oceanic whitecap coverage dependence on wind speed," *J. Phys. Oceanogr.*, Vol. 10, No. 12, 2094–2099, 1980.
34. Fung, A. K. and K. K. Lee, "A semi-empirical sea-spectrum model for scattering coefficient estimation," *IEEE Journal of Oceanic Engineering*, Vol. 7, 166–176, 1982.
35. Yang, W., Z. Zhao, C. Qi, W. Liu, and Z.-P. Nie, "Iterative hybrid method for electromagnetic scattering from a 3-D object above a 2-D random dielectric rough surface," *Progress In Electromagnetics*

Research, Vol. 117, 435–448, 2011.

36. Bausssard, A., M. Rochdi, and A. Khenchaf, "PO/MEC-based scattering model for complex objects on a sea surface," *Progress In Electromagnetics Research*, Vol. 111, 229–251, 2011.
37. Ando, M., T. Murasaki, and T. Kinoshita, "Elimination of false singularities in GTD equivalent edge currents," *IEE Proceedings H Microwaves, Antennas and Propagation*, Vol. 138, 289–296, 1991.
38. Walker, D., "Experimentally motivated model for low grazing angle radar doppler spectra of the sea surface," *IEE Proceedings — Radar, Sonar and Navigation*, Vol. 147, 114–120, 2000.
39. Toporkov, J. V. and G. S. Brown, "Numerical simulations of scattering from time-varying, randomly rough surfaces," *IEEE Trans. Geosci. Remote Sens.*, Vol. 38, No. 4, 1616–1625, 2000.
40. Plant, W. J., "Microwave sea return at moderate to high incidence angles," *Waves in Random and Complex Media*, Vol. 13, No. 4, 339–354, 2003.
41. Hwang, P. A., M. A. Sletten, and J. V. Toporkov, "Breaking wave contribution to low grazing angle radar backscatter from the ocean surface," *J. Geophys. Res.*, Vol. 113, No. C09017, 1–12, 2008.
42. Smith, T. L., T. Waseda, and C.-K. Rheem, "Measurements of the doppler spectra of breaking waves," *IET Radar Sonar Navig.*, Vol. 1, No. 2, 149–157, 2007.